ACS APPLIED BIO MATERIALS

www.acsabm.org Article

In Situ 3D-Printing using a Bio-ink of Protein−photosensitizer Conjugates for Single-cell Manipulation

Akihiro Nishiguchi, Gent Kapiti, J. Robin Höhner, Smriti Singh, and Martin Moeller*

Cite This: *ACS Appl. Bio Mater.* 2020, 3, 2378−2384 Read Online

ACCESS | Metrics & More | Article Recommendations | Supporting Information

ABSTRACT: Living tissues dynamically modulate their structure and functions through physical and biochemical interactions in the three-dimensional (3D)-microenvironment for their homeostasis or the developmental process of an embryo. However, the manipulation of cellular functions in vitro is still challenging due to the lack of a dynamic material system that can vary the 3D-cellular microenvironment in time and space. Here, we show an in situ 3D-printing technique based on multiphoton lithography using a biocompatible photoresist, bio-ink. The bio-ink composed of protein−photosensitizer conjugates has the ability to cause singlet oxygen and cross-linking reaction to fabricate protein gels with submicrometer-scale precision. Remarkably, the conjugates substantially improve the cytocompatibility and the efficiency of gelation due to the stealth effect of rose bengal (RB) and efficient transfer of singlet oxygen to bovine serum albumin (BSA). 3D-printing in the presence of cells allows for the microfabrication of a protein scaffold and controlled single-cell behavior. This dynamic material system to direct cell fate may offer emerging applications for drug discovery and regenerative medicine.

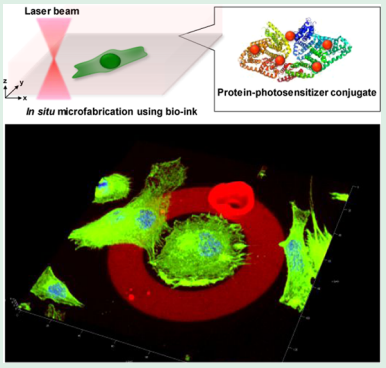

KEYWORDS: *cell manipulation, 3D-printing, photosensitizer, protein conjugate, hydrogel*

INTRODUCTION

The physical and biochemical properties of three-dimensional (3D)-cellular microenvironments dynamically regulate cell fate, tissue morphogenesis, regeneration, and homeostasis with temporal and spatial complexity.[1] For example, matrix stiffness directs the differentiation of stem cells and the patterning of signals promotes cell migration.[2−5] A mechanistic understanding of the cell−material interaction provides crucial insights to control cell fates toward drug discovery and regenerative medicine.[6] Despite great progress of synthetic materials such as hydrogels, fibers, and porous scaffolds,[7] cell manipulation in vitro is still challenging because these materials are designed to be static and show little a dynamic change in material properties such as stiffness, geometry, and biochemical signaling in time and space. The biological system is dynamic and adaptive, e.g., developmental process, and tissues vary structures and functions through cell−cell and cell−extracellular matrix (ECM) interactions.[8] A concept of dynamic biomaterial that can rebuild 3D-cellular microenvironments in the presence of cells in a time-dependent manner is an emerging approach for in situ cell manipulation.[9] Although the attempts to tune material stiffness via metal ions or UV irradiation and to pattern biomolecules using photochemistry during cell culture have been reported,[9−13] these methods suffer from the multistep process, low spatial resolution, poor dynamic modulation, and difficulty to control cell fate.

Multiphoton lithography (MPL), which is also known as direct laser writing, substantially improves the fabrication process of 3D-micro/nanostructures.[14] Due to the nonlinearity of the multiphoton absorption process, the polymerization/cross-linking reaction is confined at a focal point, allowing for 3D-printing of hydrogels at a submicrometer-scale spatial resolution.[15−17] MPL-based 3D-printing provides a new class of the bottom-up approach for in situ microfabrication, which is distinguished by conventional patterning methods to encapsulate cells in the gels.[9−13] So far, there are few reports on in situ microfabrication by MPL using a photosensitizer to cross-link proteins or photo-crosslinkable polymers.[18−21] However, a photosensitizer shows strong cytotoxicity, and only very low concentration or short time exposure was available for MPL. Moreover, these methods lack the spatiotemporal control of cell behaviors.

Here, we report a dynamic approach for cell manipulation by in situ microfabrication using a bio-ink. We newly synthesized a highly biocompatible bio-ink composed of a protein−photosensitizer conjugate. The commonly used photosensitizer, rose bengal (RB) was conjugated to bovine serum albumin (BSA) under mild conditions (Figure 1a). When exposed to a laser beam, two-photon excitation occurs at RB

Received: January 31, 2020
Accepted: March 31, 2020
Published: March 31, 2020

https://dx.doi.org/10.1021/acsabm.0c00116
ACS Appl. Bio Mater. 2020, 3, 2378−2384

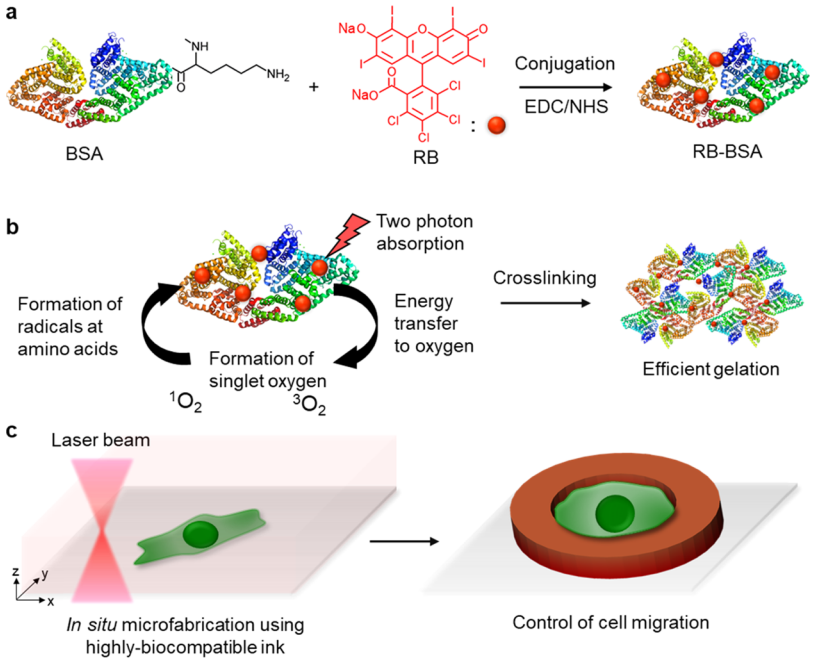

Figure 1. In situ microfabrication using a bio-ink. (a) Conjugation of rose bengal (RB) to BSA through the 1-ethyl-3-(3-dimethylaminopropyl) carbodiimide/*N*-hydroxysuccinimide (EDC/NHS) reaction. (b) When RB was excited by two-photon absorption, singlet oxygen was formed through energy transfer to oxygen, resulting in the radical formation at amino acids in protein and the cross-linking reaction between proteins. (c) MPL-based 3D-printing in the presence of cells using a biocompatible bio-ink for the control of cell functions.

and then singlet oxygen is produced through energy transfer to oxygen molecules (Figure 1b). Singlet oxygen causes radicals at amino acids of BSA, followed by cross-linking between BSA and gelation. It is expected that the conjugation of RB to BSA reduce the cytotoxicity due to the stealth effect and promote the efficiency of the gelation reaction by the close distance between RB and BSA. We addressed the ability of a bio-ink for MPL and 3D-printing in the presence of cells for the control of cell migration. This method would serve as an emerging manufacturing technology for the spatiotemporal, remote control of cell fate at a single-cell level.

MATERIALS AND METHODS

Synthesis of a Protein-Photosensitizer Conjugate. For in situ microfabrication using MPL, a protein−photosensitizer conjugate was synthesized by EDC/NHS chemistry. EDC/NHS allowed for the activation of the carboxylic groups of RB, followed by the attack of the amino groups of BSA for the conjugation. The number of photosensitizers per protein was varied by changing the molar ratio of the photosensitizer. The 0.03, 0.1, 0.25, and 0.5 equiv. rose bengal (RB, Sigma-Aldrich, USA) to bovine serum albumin (BSA, M_w = 67 kDa, Sigma-Aldrich, USA) was dissolved in phosphate-buffered saline (PBS, pH = 7.4). The 1-ethyl-3-(3-dimethylaminopropyl) carbodiimide (EDC) and *N*-hydroxysuccinimide (NHS, Sigma-Aldrich, USA) were added to the solution. BSA was dissolved in PBS at 37 °C and cooled down to room temperature. The BSA solution was added and stirred at room temperature for 24 h. The obtained conjugates were purified by dialysis in deionized water using a dialysis membrane with 3 kDa molecular weight cutoff (Spectrum Labs, USA) to remove unreacted molecules. After 3 days of dialysis, the solution was freeze-dried to obtain BSA−RB conjugates.

UV−Vis Spectroscopy. To confirm the conjugation of RB to BSA, the absorbance of the conjugates was measured by UV−vis spectroscopy (BioTek, Germany). BSA, RB, and BSA−RB conjugates dissolved in PBS were placed in a 96-well plate, and absorbance at 550 nm was measured. To quantify the number of RB molecules conjugated to the BSA molecule, the absorbance of each conjugate (BSA-RB0.5, 0.25, 0.1, 0.03) at 550 nm was measured, and the number of conjugated RB was calculated from a calibration curve of RB.

The number of RB per BSA (RB/BSA ratio) was determined using UV−vis spectroscopy by measuring the absorbance of RB in the conjugates at 548 nm ($A_{l_{max}}$) and the absorbance of proteins in the conjugates at 280 nm (A_{280}).[22] The absorption of the conjugate at 280 nm must be corrected for the contribution of RB to obtain the correct protein concentration. The RB/BSA ratio was calculated according to the following equations.

$$C_d = A_{l\max}/e_d \quad (1)$$

$$F = A_{d(280)}/A_d \quad (2)$$

$$C_p = [A_{280} - (A_{l\max}F)]/e_p \quad (3)$$

$$\mathrm{RB/BSA} = C_d/C_p \quad (4)$$

where e_d is the molar extinction coefficient of free dye (RB) at l_{max}, A_d is the absorbance of free dye at l_{max}, $A_{d(280)}$ is the absorbance of free dye at 280 nm, $A_{l_{max}}$ is the absorbance of dye in conjugate at l_{max}, e_p is the extinction coefficient of protein at 280 nm, A_{280} is the absorbance of protein in conjugate at 280 nm, C_d is the concentration of dye in conjugate (mol/L), and C_p is the concentration of protein in conjugate (mol/L). The molar extinction coefficient for BSA at 280 nm and for RB at 550 nm is approximately 43 824 and 80 000 M^{-1} cm^{-1}, respectively (Thermo Fischer Scientific).

Matrix-Assisted Laser Desorption Ionization-Time of Flight (MALDI-ToF) Mass Spectrometry. The mass analysis was performed by MALDI-TOF on a Bruker UltrafleXtreme equipped with a 337 nm smart beam laser in the linear mode. TA50 solutions (50:50 (v/v) acetonitrile/TFA 0.1% in water) of 3,5-dimethoxy-4-hydroxycinnamic acid (Sinapinic acid, 20 μL of a 20 mg/mL solution) and analyte (5 μL of a 10 mg/mL solution) were mixed and a droplet was applied on the sample target. For spectra, 4000 laser shots with 45% laser power were collected. The laser repetition rate was 1000 Hz.

https://dx.doi.org/10.1021/acsabm.0c00116
ACS Appl. Bio Mater. 2020, 3, 2378−2384

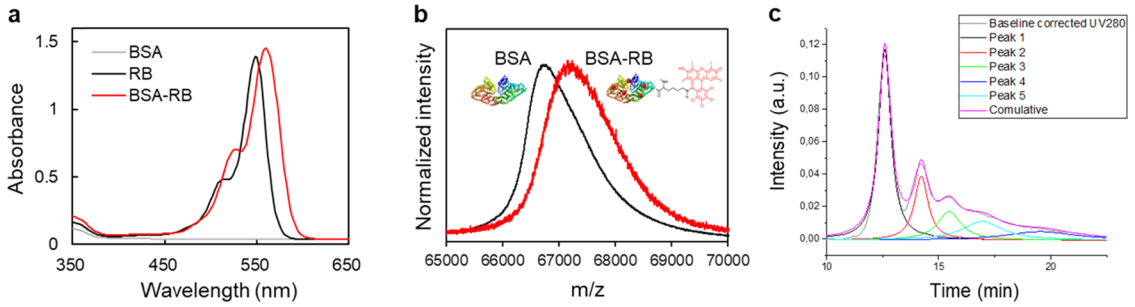

Figure 2. Characterization of protein−photosensitizer conjugates. (a) UV−vis spectroscopy of BSA, RB, and BSA−RB(2) conjugates. (b) MALDI-TOFMS measurement of BSA and BSA−RB(2) conjugates. (c) AF4 measurement of BSA−RB(2) with five Lorentzian fits to form the fit (pink).

Asymmetrical Flow Field-Flow Fractionation (AF4) Analysis. AF4 experiments were carried out using the AF2000 MT Field-Flow Fractionation of Postnova Analytics. The analyte was detected using a PN3211 UV detector (280 and 223 nm wavelength), a PN3621 MALLS detector (21 angles and wavelength of 633 nm), and a PN3150 Refractive Index Detector. A 0.9% aqueous NaCl solution was used as an eluent. The sample was dissolved in PBS with a concentration of 1 mg/mL. A 10 kDa RC membrane was used. The injection flow was adjusted to 0.2 mL/min. The detector flow was 1.0 mL/min. The separation was performed with 4.0 mL/min crossflow. The fractogram was fitted with five Lorentzian functions. The first three peaks were related to the monomer (Peak 1), dimer (Peak 2), and trimer signal (Peak 3). This assumption was underlined by comparing the results with BSA. The slow decay tends to belong to larger agglomerates. The Lorentzian functions were related according to the area underneath. An equal absorbance behavior of different sized agglomerates was assumed.

Detection of Singlet Oxygen. The production of singlet oxygen from RB in the conjugates was measured using a singlet oxygen detection probe (E_x/E_m = 504/525, singlet oxygen sensor green, Thermo Fisher Scientific). Approximately 0.4 mM RB and 14.4 mg/mL of BSA−RB(2) conjugate containing 0.4 mM RB were dissolved in PBS, and a detection probe was added at 0.02 nM. The mixture of 14 mg/mL of BSA and 0.4 mg/mL of RB was also prepared as a control. These solutions were placed in a cell and exposed to UV irradiation for 30−180 min, and the fluorescence spectrum was measured at each time point by fluorescence spectroscopy (Shimazu) when excited at λ = 504 nm.

Confocal Laser Scanning Microscopy (CLSM) and Electron Microscopy. The gels of BSA−RB were observed by confocal laser scanning microscopy (CLSM, Leica TCS SPE, Leica, Germany), and the obtained images were analyzed using LAS AF Lite (Leica, Germany). Scanning electron microscopy (SEM) was used with an S-4800 ultrahigh-resolution SEM (HITACHI, Japan). The samples were coated with a 6 nm thick gold film by spattering for the observation. The accelerating voltage and working distance were set to 5 kV and 10−15 mm, respectively.

Cytotoxicity Assay. The protein, photosensitizer, and BSA−RB conjugate were dissolved in the cell culture medium at 37 °C. Before use, the solution was filtrated with a 0.2 mm syringe filter (Whatman, USA). L929 mouse fibroblast cells were cultured in the Dulbecco's modified Eagle's medium (DMEM) medium (Sigma-Aldrich, USA) containing 10% Fetal bovine serum (FBS) (Thermo Fisher Scientific, USA) and 1% penicillin/streptomycin (Sigma-Aldrich, USA) in a 5% CO_2 incubator at 37 °C. L929 cells were harvested using trypsin, and the cell number was counted by the trypan blue exclusion assay. A total of 1×10^4 L929 cells were seeded into a 96-well plate. After the cultivation overnight, the media were removed from the plates, and 200 mL of each solution was added to the plate. The cells were incubated for 1 h at room temperature under light-shielding conditions to prevent the generation of reactive oxygen species. After 1 h, cells were washed three times with PBS and incubated in 200 mL of media overnight in a 5% CO_2 incubator at 37 °C. To evaluate the cell viability, an XTT assay kit (AppliChem, US) was used. Briefly, 50 mL of XTT reagents were added to each well, and the samples were incubated for 2 h. The absorbance of media at 450 nm was then measured by a plate reader. The cell number was calculated from a standard curve.

In Situ Microfabrication by MPL. As a chamber, sterile round-shaped poly(dimethylsiloxane) (PDMS) mold (outer dimension: 2 cm in diameter, inner dimension: 1 cm in diameter) was placed on a coverslip (30 mm in diameter, 0.13−0.16 mm in thickness) and put in a 6-well plate. A total of 1×10^3 L929 cells were seeded into a chamber. After 1 h of incubation, 4 mL of media were added into a well plate and the sample was cultured for 24 h. For the MPL experiment, the culture medium in a chamber was removed and a photoresist of BSA−RB conjugates was added. Before use, the photoresist was filtrated with a 0.2 mm syringe filter to remove dust and aggregation. To avoid drying of the cells, the chamber was covered with a (15 × 15) mm coverslip. The MPL process was performed using the Photonic Professional DLW system (Nanoscribe GmbH, Germany) with an oil-immersion 63× objective lens (numerical aperture (NA): 1.4, Zeiss, Germany). The femtosecond laser (emission wavelength: 780 nm, pulse width: 120 fs, and repetition rate: 100 MHz) was used as a laser source. The structures were designed using computer-aided design software (AutoCAD, Autodesk, CA), and a virus-like structure model was obtained from the NIH 3D Print Exchange. A laser power of 50 mW and scanning speed of 1000 mm s^{-1} were used for MPL, and the hatching/slicing distance was set to 300 nm.

Fluorescence Staining. The cells were fixed with 4% paraformaldehyde (PFA) for 15 min and washed with PBS. The samples were treated with 0.2% Triton-X for 15 min for permeabilization. After washing with PBS, the cells were incubated with 5% BSA and 5% goat serum/PBS for 1 h for blocking. The cells were then incubated with phalloidin with the Alexa 488 (Thermo Fisher Scientific, USA)/1% BSA solution for 1 h. After washing with PBS, nuclei were stained with 4′,6-diamidino-2-phenylindole dihydrochloride (DAPI, Thermo Fisher Scientific). The samples were observed by CLSM.

Statistical Analysis. All data were expressed as means ± standard deviation (SD) from three independent experiments unless otherwise specified. A p value < 0.05 was considered to be statistically significant.

RESULTS AND DISCUSSION

Preparation and Characterization of Protein-Photosensitizer Conjugates. To develop a biocompatible photoresist, we synthesized protein−photosensitizer conjugates. The most abundant plasma protein, BSA, was selected because of the high solubility in water, unlike other proteins such as collagen. BSA was conjugated with RB through carbodiimide and *N*-hydroxysuccinimide (EDC/NHS) chemistry.[22] The carboxylic groups of RB were activated by EDC/NHS and reacted with the amines of BSA, which possess 30 reactive lysines per molecule (59 lysines in total). By changing the feed ratio of RB in a range of 0.03−0.5 equiv. to BSA, the conjugates with various number of RB per BSA molecule were

https://dx.doi.org/10.1021/acsabm.0c00116
ACS Appl. Bio Mater. 2020, 3, 2378−2384

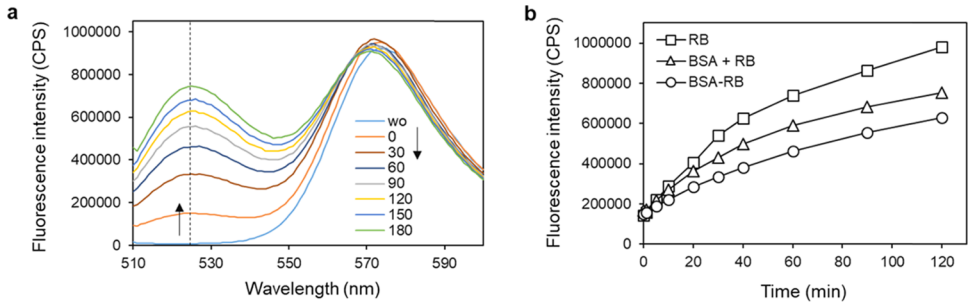

Figure 3. Production of singlet oxygen. (a) Fluorescence spectroscopy of BSA−RB(2) with a singlet oxygen detection probe (E_m = 525 nm) when exposed to UV irradiation for 30−180 min. (b) Fluorescence intensities at 525 nm of RB, BSA + RB, and BSA−RB(2) as a function of time.

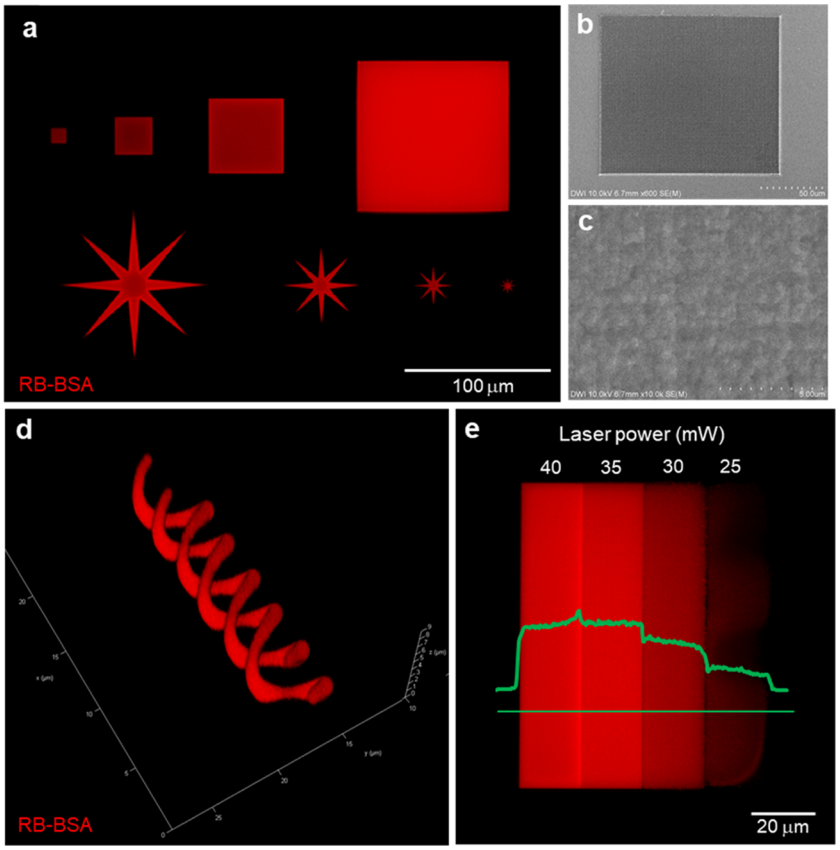

Figure 4. 3D-printing of protein gels and optimization of printing conditions. (a) CLSM image and (b, c) SEM images of 10−100 μm cubic or star-shaped hydrogel films using the BSA−RB(2) conjugate. (d) CLSM image of 3D-double helix structures of protein gels. (e) CLSM image of cuboid structures prepared by different laser powers ranging from 25 to 40 mW.

synthesized. The number of RB in conjugate was determined to be 1, 2, 3, and 5 (called BSA−RB(1), BSA−RB(2), BSA−RB(3), and BSA−RB(5)), respectively by UV−vis spectroscopy (Table S1). We confirmed the conjugation of RB to BSA in BSA−RB(2) from UV−vis spectroscopy, and FT-IR and the slight red shift was observed after the conjugation due to the change of the conjugate structure in RB (Figures 2a and S1). Matrix-assisted laser desorption ionization time of flight mass spectrometry (MALDI-TOFMS) shows the peak shift in the conjugates, and the molecular weights of BSA and BSA−RB(2) were estimated to be 66 700 and 67 200 Da from peak values, respectively (Figure 2b). Although the peak difference was smaller than the theoretical value due to the broad distribution, it depicts the conjugation of RB via chemical bonding. Due to the activation of the carboxylic group on proteins, multimerization by cross-linking between the proteins may occur. We confirmed by asymmetrical flow field-flow fractionation (AF4) analysis that BSA−RB(2) conjugates contained 46% monomer, 17% dimer, 13% trimer, and 24% larger agglomerates (Figure 2c).

To investigate the role of singlet oxygen in protein cross-linking, the production of singlet oxygen was analyzed. Due to the formation of a reactive triplet state of a photosensitizer after the excitation, the photosensitizer undergoes energy transfer to oxygen to form singlet oxygen,[23] which results in cross-linking of proteins such as tyrosine and tryptophan.[24] A fluorescence probe that emits fluorescence at 525 nm by the reaction with singlet oxygen was employed for the detection (E_m/E_x = 504/525 nm). Figure 3a represents a fluorescence spectrum of a bio-ink of RB-BSA(2) containing the probe when it was exposed to UV irradiation at 340 nm alternative to two-photon excitation by a λ = 780 nm laser. With the increase

https://dx.doi.org/10.1021/acsabm.0c00116
ACS Appl. Bio Mater. 2020, 3, 2378−2384

of exposure time, the fluorescence intensity at 525 nm increased, indicating the production of singlet oxygen. The spectrum around 575 nm arising from RB shows no change after the irradiation. Interestingly, compared to only RB or the mixture of RB and BSA in water, less singlet oxygen was observed in BSA−RB(2) (Figure 3b). This result indicates that in the presence of BSA, singlet oxygen produced by RB was consumed by the amino acids in BSA, and the conjugates possessing the functions as "initiator" and "monomer" allow efficient transfer of singlet oxygen to amino acids due to close distance compared to the mixture of BSA and RB.

3D-Printing of Protein Gels by MPL. Next, we addressed MPL-based 3D-printing of protein gels using a bio-ink comprising the BSA−RB conjugate. As explained above, proteins can photoresist in the presence of a suitable photosensitizer. The formed singlet oxygen causes a radical at amino acids in proteins such as tryptophan and tyrosine, resulting in cross-linking with other proteins and the gelation reaction.[15−17] Even though RB does not have strong absorption around 390 nm, which is necessary for two-photon excitation by a λ = 780 nm pulsed laser, RB can be used as a photosensitizer for hydrogel fabrication. The bio-ink on a coverslip was placed on the stage of MPL with a femtosecond laser, a 3D-piezo scanning stage, and an oil-immersion 63× objective lens (numerical aperture: 1.4). Tightly focused laser beams elicited the photo-cross-linking of proteins at the focal point to form protein gels. Confocal laser scanning microscope (CLSM) observation displayed successful fabrication of 10−100 μm sized cubic or star-shaped hydrogel films, as designed, using BSA−RB(2) conjugates (Figure 4a). Protein gels did not show swelling during the printing process. SEM observation shows a sharp-edge and smooth surface as designed, and printing with submicrometer-scale precision was achieved (Figure 4b,c). Moreover, MPL allowed for the fabrication of a more complex 3D-structure of protein gels, double helix, using this bio-ink (Figure 4d). The physical property of gels, such as stiffness, can be tuned by the writing condition (laser power and scanning speed) and design (distance between focal points). The variation of laser power in a range of 25−40 mW resulted in the formation of gels with controlled material density (Figure 4e).

Biocompatibility of the Bio-Ink. The most crucial point of in situ fabrication using a protein−photosensitizer photoresist is a balance between cytotoxicity and gelation. Since a photosensitizer causes cytotoxicity at high concentration, it needs to be used at low concentration or for a short exposure time. However, the gelation reaction does not proceed at a low concentration of the photosensitizer, and the trade-off needs to be considered. Although several photoinitiators or photosensitizers are available for the MPL system,[25] in fact, commonly used photosensitizers, RB and methylene blue, show strong toxicity to L929 fibroblasts at more than 100 μM for 1 h of incubation even under light-shielding conditions (Figures 5a and S2). BSA was highly cytocompatible even at a high concentration (400 mg/mL). A water-soluble photoinitiator, I2959, has been used as a cytocompatible photoinitiator for 3D-bioprinting but did not allow for gelation in this system due to low absorption at 390 nm. We evaluated the cytocompatibility of BSA−RB conjugates with different modification numbers ranging from 5 to 1. The cytocompatibility of the conjugates to L929 fibroblasts increased with decreasing modification number. The maximum concentration of the conjugates (mg/mL) at which they show more than 90%

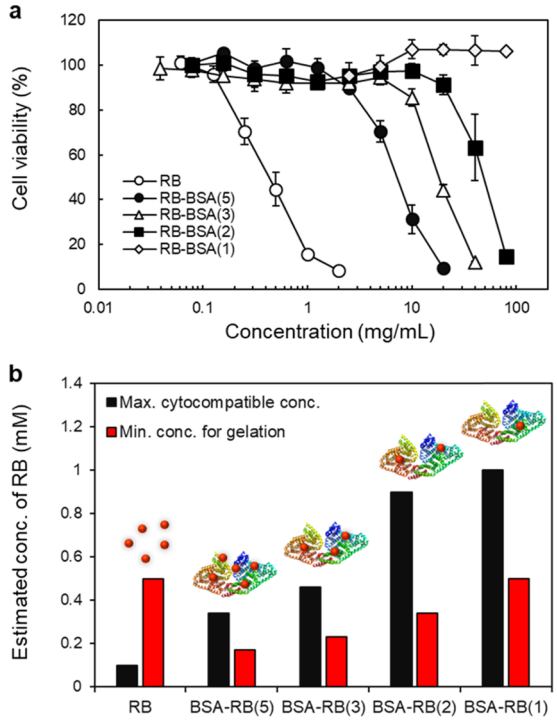

Figure 5. Biocompatibility of a bio-ink. (a) Cell viability when exposed to bio-inks comprising free RB, BSA−RB(5), (3), (2), and (1) for 1 h. The viability of L929 fibroblasts was evaluated by a colorimetric assay using formazan (XTT assay). (b) Maximum applicable biocompatible concentration of RB in bio-inks and minimum concentration necessary for the gelation reaction.

cell viability was determined from Figure 4a, and the concentrations of RB contained in the conjugates (mM) were estimated. As shown in Figure 5b, the maximum cytocompatible concentration of the BSA−RB(2) conjugate was determined as 0.9 mM, and the cytocompatibility of the bio-ink was substantially improved by this conjugation system compared to free RB (0.25 mM). The conjugation of RB to BSA increased the molecular weight more than 60 times and the hydrophilicity, which may reduce the uptake by cells (stealth effect). To check whether these concentrations of conjugates can induce gelation, we printed cubic structures with the formation of the structures. While the bio-ink of free RB required 0.5 mM for the fabrication of the structure, the bio-ink composed of the BSA−RB(5) conjugate achieved gelation at 0.17 mM. Among the bio-inks of the conjugates, the minimum concentration of RB decreased with the increase in the modification number. Thus, remarkably, the conjugation system also contributed to improving the gelation reaction compared to free RB. It is explained that the localization of the photosensitizer in BSA−RB(5) efficiently promotes the transfer of singlet oxygen to BSA and the gelation process, as shown in Figure 2e. Taken together, BSA−RB conjugates improve both cytocompatibility and gelation reaction, and in the case of BSA−RB(2), the range between the maximum biocompatible concentration and the minimum concentration necessary for gelation was 0.34−0.9 mM, which is the applicable concentration for in situ microfabrication. On the other hand, free RB required higher concentration than the cytocompatible range and cannot be used for MPL in the presence of cells. This conjugation system led to the

https://dx.doi.org/10.1021/acsabm.0c00116
ACS Appl. Bio Mater. 2020, 3, 2378−2384

development of biocompatible bio-inks for in situ cell manipulation.

In Situ 3D-Printing for Cell Manipulation. Finally, we performed in situ 3D-printing using the bio-ink of BSA−RB conjugates. L929 fibroblasts were cultured on a coverslip with a PDMS chamber for 1 day, and then 20 mg/mL of BSA−RB(2) conjugate ink was added. A ring-shaped structure with 60 μm inner diameter and 100 μm outer diameter was printed around a cell (Figure 6a). The cell shows no change in the morphology

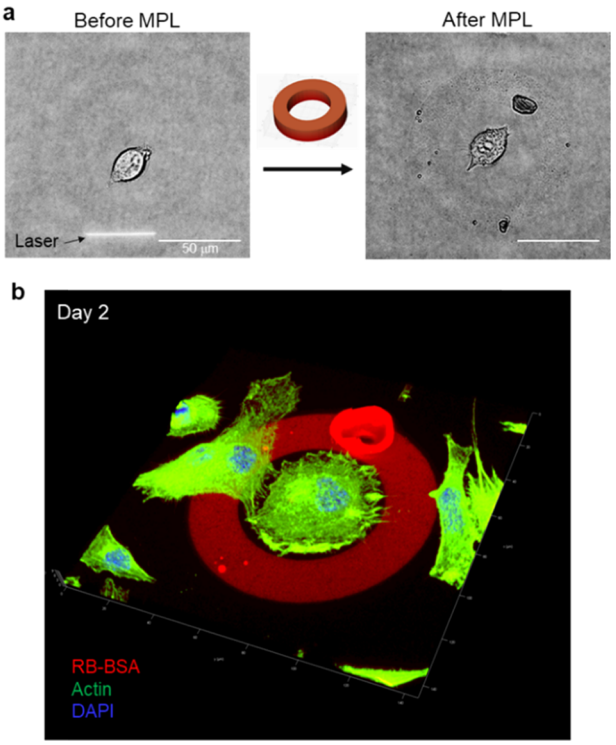

Figure 6. In situ 3D-printing for the control of single-cell behavior. (a) Phase-contrast images of a ring structure with 60 μm inner diameter and 100 μm outer diameter and a fibroblast cell before and after the printing process; 20 mg/mL of BSA−RB(2) conjugates were used. (b) 3D-reconstructed CLSM image of cells cultured for 2 days in a printed structure. After in situ printing, the cells started to spread and migrate but stayed in a ring structure. Actin was stained with fluorescently-labeled phalloidin (green). Nuclei were stained with DAPI (blue).

after the printing process. After cells were washed with PBS and cultured for 2 days, the cell surrounded by the ring structure still stayed in it (Figure 6b). Although cells started to spread and migrate as usual, the printed structure limited the cell migration to outside, indicating that in situ 3D-printing controlled the cell behavior at a single-cell level. We also observed stiffness-dependent[26] cell adhesion on gels prepared using BSA−RB(2) conjugates although the gels were prepared before the seeding of cells (Figure S3). Tuning hatching/slicing distance can change the density of printing networks in hydrogels and the stiffness of hydrogels.[27] The accurate control of the cellular microenvironment, especially in the presence of cells, would contribute to understanding cell functions. For further advances, the development of advanced technology that can modulate matrix stiffness,[28,29] topologically guide the migration,[30,31] pattern biomolecules,[32,33] combine with cell encapsulation in bioprinting[34] would be a key challenge to direct cell fate.

CONCLUSIONS

In conclusion, we reported in situ microfabrication technique based on the MPL system using a biocompatible photoresist composed of protein−photosensitizer conjugates. BSA−RB conjugates have the ability to cause singlet oxygen and the cross-linking reaction to fabricate protein gels. Remarkably, the conjugates substantially improved the cytocompatibility and the efficiency of gelation depending on the modification number of RB due to the stealth effect of RB and the efficient transfer of singlet oxygen to BSA. 3D-printing in the presence of cells allowed for the dynamic modulation of single-cell behavior at a submicrometer-scale spatial resolution. In principle, this method is applicable for any type of ECM proteins instead of BSA. Since hydrogel scaffolds composed of ECM proteins such as gelatin and elastin exhibit excellent biocompatible and cell-adhesive properties,[35] the use of ECM proteins enables us to fabricate more functional scaffolds in terms of mechanical strength and biochemical signals. This dynamic material system to direct cell fate may offer emerging applications for drug discovery and regenerative medicine.

ASSOCIATED CONTENT

Supporting Information

The Supporting Information is available free of charge at https://pubs.acs.org/doi/10.1021/acsabm.0c00116.

Summary of the property of BSA−RB conjugates; FT-IR spectroscopy; toxicity assays; cellular adhesion test on hydrogels (PDF)

AUTHOR INFORMATION

Corresponding Author

Martin Moeller − *DWI—Leibniz-Institute for Interactive Materials, D-52056 Aachen, Germany;* orcid.org/0000-0002-5955-4185; Email: moeller@dwi.rwth-aachen.de

Authors

Akihiro Nishiguchi − *DWI—Leibniz-Institute for Interactive Materials, D-52056 Aachen, Germany;* orcid.org/0000-0002-3160-6385

Gent Kapiti − *DWI—Leibniz-Institute for Interactive Materials, D-52056 Aachen, Germany*

J. Robin Höhner − *DWI—Leibniz-Institute for Interactive Materials, D-52056 Aachen, Germany*

Smriti Singh − *DWI—Leibniz-Institute for Interactive Materials, D-52056 Aachen, Germany;* orcid.org/0000-0002-2164-9912

Complete contact information is available at: https://pubs.acs.org/10.1021/acsabm.0c00116

Notes

The authors declare no competing financial interest.

ACKNOWLEDGMENTS

This work was supported by SFB 985-Functional Microgels and Microgel Synthesis, the ERC Advanced Grant 695716, and the Center for Chemical Polymer Technology supported by the EU and the state of North Rhine-Westphalia (Grant No. EFRE 30 00 883 02).

REFERENCES

(1) Lutolf, M. P.; Hubbell, J. A. Synthetic biomaterials as instructive extracellular microenvironments for morphogenesis in tissue engineering. *Nat. Biotechnol.* **2005**, *23*, 47−55.

(2) Engler, A. J.; Sen, S.; Sweeney, H. L.; Discher, D. E. Matrix elasticity directs stem cell lineage specification. *Cell* **2006**, *126*, 677−689.

(3) Huebsch, N.; Arany, P. R.; Mao, A. S.; Shvartsman, D.; Ali, O. A.; Bencherif, S. A.; Rivera-Feliciano, J.; Mooney, D. J. Harnessing traction-mediated manipulation of the cell/matrix interface to control stem-cell fate. *Nat. Mater.* **2010**, *9*, 518−526.

(4) Luo, Y.; Shoichet, M. S. A photolabile hydrogel for guided three-dimensional cell growth and migration. *Nat. Mater.* **2004**, *3*, 249−253.

(5) Lee, S. H.; Moon, J. J.; West, J. L. Three-dimensional micropatterning of bioactive hydrogels via two-photon laser scanning photolithography for guided 3D cell migration. *Biomaterials* **2008**, *29*, 2962−2968.

(6) Place, E. S.; Evans, N. D.; Stevens, M. M. Complexity in biomaterials for tissue engineering. *Nat. Mater.* **2009**, *8*, 457−470.

(7) Peppas, N. A.; Hilt, J. Z.; Khademhosseini, A.; Langer, R. Hydrogels in biology and medicine: from molecular principles to Bionanotechnology. *Adv. Mater.* **2006**, *18*, 1345−1360.

(8) Thiery, J. P.; Acloque, H.; Huang, R. Y. J.; Nieto, M. A. Epithelial-mesenchymal transitions in development and disease. *Cell* **2009**, *139*, 871−890.

(9) Kloxin, A. M.; Kasko, A. M.; Salinas, C. N.; Anseth, K. S. Photodegradable hydrogels for dynamic tuning of physical and chemical properties. *Science* **2009**, *324*, 59−63.

(10) Gillette, B. M.; Jensen, J. A.; Wang, M.; Tchao, J.; Sia, S. K. Dynamic hydrogels: switching of 3D microenvironments using two-component naturally derived extracellular matrices. *Adv. Mater.* **2010**, *22*, 686−691.

(11) Khetan, S.; Guvendiren, M.; Legant, W. R.; Cohen, D. M.; Chen, C. S.; Burdick, J. A. Degradation-mediated cellular traction directs stem cell fate in covalently crosslinked three-dimensional hydrogels. *Nat. Mater.* **2013**, *12*, 458−465.

(12) Mosiewicz, K. A.; Kolb, L.; van der Vlies, A. J.; Martino, M. M.; Lienemann, P. S.; Hubbell, J. A.; Ehrbar, M.; Lutolf, M. P. In situ cell manipulation through enzymatic hydrogel photopatterning. *Nat. Mater.* **2013**, *12*, 1072−1078.

(13) DeForest, C. A.; Anseth, K. S. Photoreversible patterning of biomolecules within click-based hydrogels. *Angew. Chem., Int. Ed.* **2012**, *51*, 1816−1819.

(14) Zhang, Y. L.; Chen, Q. D.; Xia, H.; Sun, H. B. Designable 3D nanofabrication by femtosecond laser direct writing. *Nano Today* **2010**, *5*, 435−448.

(15) Pitts, J. D.; Campagnola, P. J.; Epling, G. A.; Goodman, S. L. Submicron multiphoton free-form fabrication of proteins and polymers: studies of reaction efficiencies and applications in sustained release. *Macromolecules* **2000**, *33*, 1514−1523.

(16) Kaehr, B.; Shear, J. B. Multiphoton fabrication of chemically responsive protein hydrogels for microactuation. *Proc. Natl. Acad. Sci. U.S.A.* **2008**, *105*, 8850−8854.

(17) Loebel, C.; Broguiere, N.; Alini, M.; Zenobi-Wong, M.; Eglin, D. Microfabrication of photo-cross-linked hyaluronan hydrogels by single- and two-photon tyramine oxidation. *Biomacromolecules* **2015**, *16*, 2624−2630.

(18) Kaehr, B.; Allen, R.; Javier, D. J.; Currie, J.; Shear, J. B. Guiding neuronal development with in situ microfabrication. *Proc. Natl. Acad. Sci. U.S.A.* **2004**, *101*, 16104−16108.

(19) Sun, Y. L.; Li, Q.; Sun, S. M.; Huang, J. C.; Zheng, B. Y.; Chen, Q. D.; Shao, Z. Z.; Sun, H. B. Aqueous multiphoton lithography with multifunctional silk-centred bio-resists. *Nat. Commun.* **2015**, *6*, 8612.

(20) Ovsianikov, A.; Mühleder, S.; Torgersen, J.; Li, Z.; Qin, X. H.; Van Vlierberghe, S.; Dubruel, P.; Holnthoner, W.; Redl, H.; Liska, R.; Stampfl, J. Laser photofabrication of cell-containing hydrogel constructs. *Langmuir* **2014**, *30*, 3787−3794.

(21) Mironi-Harpaz, I.; Hazanov, L.; Engel, G.; Yelin, D.; Seliktar, D. In-situ architectures designed in 3D cell-laden hydrogels using microscopic laser photolithography. *Adv. Mater.* **2015**, *27*, 1933−1938.

(22) Brinkley, M. A brief survey of methods for preparing protein conjugates with dyes, haptens and crosslinking reagents. *Bioconjugate Chem.* **1992**, *3*, 2−13.

(23) Bonnett, R. Photosensitizers of the porphyrin and phthalocyanine series for photodynamic therapy. *Chem. Soc. Rev.* **1995**, *24*, 19−33.

(24) Webster, A.; Britton, D.; Apap-Bologna, A.; Kemp, G. A dye-photosensitized reaction that generates stable protein-protein cross-links. *Anal. Biochem.* **1989**, *179*, 154−157.

(25) Torgersen, J.; Qin, X. H.; Li, Z.; Ovsianikov, A.; Liska, R.; Stampfl, J. Hydrogels for two-photon polymerization: A toolbox for mimicking the extracellular matrix. *Adv. Funct. Mater.* **2013**, *23*, 4542−4554.

(26) Khripin, C. Y.; Brinkerabc, C. J.; Kaehr, B. Mechanically tunable multiphoton fabricated protein hydrogels investigated using atomic force microscopy. *Soft Matter* **2010**, *6*, 2842−2848.

(27) Nishiguchi, A.; Zhang, H.; Schweizerhof, S.; Friederike Schulte, M.; Mourran, A.; Möller, M. 4D-printing of light-driven soft actuator with programmed printing density. *ACS Appl. Mater. Interfaces* **2020**, *12*, 12176−12185. DOI: 10.1021/acsami.0c02781.

(28) Discher, D. E.; Janmey, P.; Wang, Y. L. Tissue cells feel and respond to the stiffness of their substrate. *Science* **2005**, *310*, 1139−1143.

(29) Mihalko, E. P.; Brown, A. C. Material strategies for modulating epithelial to mesenchymal transitions. *ACS Biomater. Sci. Eng.* **2018**, *4*, 1149−1161.

(30) Casanova, A.; Blatche, M. C.; Ferre, C. A.; Martin, H.; Gonzalez-Dunia, D.; Nicu, L.; Larrieu, G. Self-aligned functionalization approach to order neuronal networks at the single-cell level. *Langmuir* **2018**, *34*, 6612−6620.

(31) Huang, Y. A.; Ho, C. T.; Lin, Y. H.; Lee, C. J.; Ho, S. M.; Li, M. C.; Hwang, E. Nanoimprinted anisotropic topography preferentially guides axons and enhances nerve regeneration. *Macromol. Biosci.* **2018**, *18*, No. 1800335.

(32) Luo, Y.; Shoichet, M. S. A photolabile hydrogel for guided three-dimensional cell growth and migration. *Nat. Mater.* **2004**, *3*, 249−253.

(33) Tam, R. Y.; Smith, L. J.; Shoichet, M. S. Engineering cellular microenvironments with photo- and enzymatically responsive hydrogels: toward biomimetic 3D cell culture models. *Acc. Chem. Res.* **2017**, *50*, 703−713.

(34) Ng, W. L.; Lee, J. M.; Zhou, M.; Chen, Y.-W.; Lee, K.-X. A.; Yeong, W. Y.; Shen, Y.-F. Vat polymerization-based bioprinting—process, materials, applications and regulatory challenges. *Biofabrication* **2020**, *12*, No. 022001.

(35) Gungor-Ozkerim, P. S.; Inci, I.; Zhang, Y. S.; Khademhosseini, A.; Dokmeci, M. R. Bioinks for 3D bioprinting: an overview. *Biomater. Sci.* **2018**, *6*, 915−946.

https://dx.doi.org/10.1021/acsabm.0c00116
ACS Appl. Bio Mater. 2020, 3, 2378−2384